

BeppoSAX Spectral Survey of soft X-ray selected BL Lacs

A. Wolter,¹ A. Comastri,² G. Ghisellini,¹ P. Giommi,³ M. Guainazzi,³ T. Maccacaro,¹ L. Maraschi,¹ P. Padovani,^{4,5,6} C.M. Raiteri,⁷ G. Tagliaferri,¹ C.M. Urry,⁴ M. Villata.⁷

¹ Osservatorio Astronomico di Brera Via Brera, 28 20121 MILANO, Italy

² Osservatorio Astronomico di Bologna, Via Zamboni 33, 40126 Bologna, Italy.

³ A.S.I., Beppo-SAX Science Data Center, Via Corolle 19, I-00131, Roma, Italy

⁴ Space Telescope Science Institute, 3700 San Martin Drive, Baltimore, MD. 21218, USA

⁵ Affiliated to the Astrophysics Division, Space Science Department, European Space Agency

⁶ On leave from Dipartimento di Fisica, II Università di Roma “Tor Vergata”, Italy

⁷ Osservatorio Astronomico di Torino, Strada Osservatorio 20, I-10025 Pino Torinese (TO), Italy

Received; accepted

Abstract. We present X-ray spectra obtained with *BeppoSAX* (Satellite per Astronomia X) of 10 BL Lac objects, selected from the Einstein Medium Sensitivity and Slew Surveys. We find that in about half of the objects a fit in the 0.1-10 keV range with a single power law and free absorption yields values of N_{H} larger than the Galactic ones. In most of these cases, however, broken power law fits with N_{H} fixed at the Galactic values yield an alternative, better description of the data and indicate a steepening of the spectrum with increasing energy. One object (1ES1101-232) is detected up to ~ 100 keV. Its spectral energy distribution (SED) peaks in the medium energy X-ray band. For each object we compute the peak frequency of the SED from multifrequency data. The spectral indices α_x in the 2-10 keV band ($F_{\nu} \propto \nu^{-\alpha_x}$) are smaller (i.e. flatter spectrum) for objects with higher peak frequencies. We therefore confirm and extend to higher energies the behavior already known for X-ray selected BL Lac objects in the ROSAT band. We do not find spectral indices smaller than 1; however, the flat distribution of α_x and the correlation between α_x and peak frequency found from our data suggest that a number of objects may exist, which in the quiescent status have flatter spectrum and peak frequency in the hard X-ray range.

Key words: (Galaxies:) BL Lacertae objects: general – X-rays: galaxies

1. Introduction

BL Lacertae objects are a rare type of Active Galactic Nuclei (AGN) characterized by strong and variable emission

Send offprint requests to: A. Wolter: anna@brera.mi.astro.it

of non-thermal radiation across the entire electromagnetic spectrum, from radio waves to high energy γ -rays. In three cases (Mkn 421: Punch et al. 1992; Mkn 501: Quinn et al. 1996; 1ES 2344+514: Catanese et al., 1998) the emission has been detected up to TeV energies. BL Lacertae objects comprise the most violent (highly and rapidly variable, highly polarized) and most elusive (extremely difficult to find in optical surveys) sources amongst AGN. Unlike most other AGN they do not show evidence (by definition) for strong emission lines or large Infra-Red or UV excesses. The emission from radio to γ -rays can be explained as due to synchrotron radiation up to a certain maximum frequency (that ranges approximately from 10^{13} to 10^{17} Hz), above which a sharp turnover occurs until a second component due to Compton scattered radiation dominates, making these objects detectable up to the highest energies so far accessible (see e.g., Ulrich, Maraschi and Urry, 1997). The extreme properties of BL Lacs require that the matter emitting the radiation moves at relativistic speeds in the direction of the observer.

The spectral change from synchrotron to Compton radiation is crucial for the understanding of the physics of BL Lacs. However, up to now this has been inferred only from the comparison of X-ray measurements carried out with different instruments and very often at different epochs. The wide energy band of *BeppoSAX* offers for the brightest objects the best opportunity to directly detect without ambiguity this spectral change and to study the X-ray spectra at the same epoch over a large interval.

To this end we have undertaken a program that aims at studying in detail the X-ray spectrum of a large and well defined subsample of soft X-ray selected BL Lacs. This sample includes mostly objects that are expected to show strong spectral curvature and spectral breaks, since the synchrotron break should occur just before or in the *Beppo-*

poSAX band. We aim at measuring in detail the shape of the most energetic part of the synchrotron emission, and trying to establish where and how the Compton component becomes dominant. We also intend to look for the correlation between spectral slope and break energy found in ROSAT data (Padovani & Giommi, 1996; Lamer, Brunner & Staubert, 1996).

2. The Sample of soft X-ray selected BL Lacs

Unlike any other type of AGNs, more than 90% of all known BL Lacs have been discovered either in radio or X-ray surveys. The former (often called RBLs) were found to show somewhat different properties from the latter (often called XBLs). From the viewpoint of the broad band spectrum the two classes differ mostly in the position of the synchrotron break with RBL showing mostly a low energy break and XBL showing the break at higher energies. A classification has recently been introduced where objects for which the break occurs at low energy (IR-Optical) are called LBLs (Low-frequency cut-off BL Lacs) and objects where the turnover occurs at higher energies (UV-X-ray) are called HBLs (High-frequency cut-off BL Lacs; see Padovani & Giommi, 1995). In this scheme most (but not all) RBL are LBL and most (but not all) XBL are HBLs.

At present, X-ray selected BL Lacs are mainly the result of surveys carried out with the *Einstein* IPC. The Slew Survey sample (Perlman et al. 1996a) covers essentially the entire high Galactic latitude sky with a rather high flux limit, while the EMSS survey (Gioia et al. 1990) is deeper than the Slew Survey but covers only ~ 800 sq.deg. of the sky, with almost two orders of magnitude better sensitivity. By selecting objects with flux [0.1–10 keV] higher than 10^{-11} erg cm $^{-2}$ s $^{-1}$ in the Slew Survey and higher than 4×10^{-12} erg cm $^{-2}$ s $^{-1}$ in the EMSS we obtain a sample that combines the advantages of a flux-limited (and therefore statistically well defined) sample with a wide coverage of the parameter space (i.e., X-ray and radio luminosity, redshift, F_x/F_r , etc.) which neither of the two surveys alone would provide.

The sample we present here includes the first 10 objects of this project observed by the Narrow Field Instruments of *BeppoSAX* and represents a significant fraction of the total sample that will be published when available. Name(s) and redshift for each source are listed in the Journal of Observations (Table 1), described in the next Section.

3. *BeppoSAX* Observations and Data Analysis

The X-ray astronomy satellite *BeppoSAX* is a project of the Italian Space Agency (ASI) with a participation of the Netherlands Agency for Aerospace Programs (NIVR). The scientific payload comprises four Narrow Field Instruments [NFI: Low Energy Concentrator Spectrometer (LECS), Medium Energy Concentrator Spectrometer

(MECS), High Pressure Gas Scintillation Proportional Counter (HPGSPC), and Phoswich Detector System (PDS)], all pointing in the same direction, and two Wide Field Cameras (WFC), pointing in opposite directions perpendicular to the NFI common axis. A detailed description of the entire *BeppoSAX* mission can be found in Butler & Scarsi (1990) and Boella et al. (1997a).

The MECS consists of three equal units, each composed of a grazing incidence mirror unit and of a position sensitive gas scintillation proportional counter, with a field of view of 56 arcmin diameter, working range 1.3–10 keV, energy resolution $\sim 8\%$ and angular resolution ~ 0.7 arcmin (FWHM) at 6 keV. The effective area at 6 keV is 155 cm 2 (Boella et al., 1997b)

The LECS is a unit similar to the MECS, with a thinner window that grants a lower energy cut-off (sensitive in the energy range 0.1–10.0 keV) but also reduces the FOV to 37 arcmin diameter (Parmar et al. 1997). The LECS energy resolution is a factor ~ 2.4 better than that of the ROSAT PSPC, while the effective area is between a factor ~ 6 and 2 lower at 0.28 and 1.5 keV, respectively.

The PDS is a system of four crystals, sensitive in the 13–200 keV band and mounted on a couple of rocking collimators, which points two units on the targets and two units 3.5° aside respectively, to monitor the background. The position of the collimators flips every 96 seconds. Thanks to the stability of the instrumental background, the PDS has shown an unprecedented sensitivity in its energy range, allowing 3σ detection of $\alpha \sim 1$ sources as faint as 10 mCrab with 10 ks of effective exposure time (Guainazzi & Matteuzzi, 1997).

As of April 1997, 10 of the scheduled X-ray selected BL Lacs have been observed; the data have been preprocessed at the *BeppoSAX* SDC (Science Data Center) and retrieved through the SDC archive. Table 1 lists a journal of the observations with the names and the known redshifts for reference, the observation date and the good-data times in the LECS and MECS, together with the extracted net counts and photon counting statistics errors. For two objects, 1ES0414+009 and 1ES0502+675, the LECS instrument was not available during the observation. For the others, the LECS exposure times are considerably reduced with respect to the MECS exposure times (a factor of 2 to 7) because the LECS can operate only when the spacecraft is not illuminated by the Sun.

3.1. Variability

Large intensity variations in the X-ray band are not uncommon for BL Lacs objects, and affect the entire spectral distribution; in a few, maybe extreme, cases of the brightest HBL observed, even variations up to 2 orders of magnitude of the position of the emission peak in the spectral energy distribution have been detected (e.g., Mkn 501: Pian et al., 1998; 1ES 2344+514: Giommi, Padovani & Perlman, 1998 and in preparation)

Table 1. Journal of Observations

Name	z	Obs. Date d/m/y	Exp. Time(sec) (LECS)	net counts (LECS)	Exp. Time(sec) (MECS)	net counts (MECS)
MS0158.5+0019	0.299	16-17/08/96	4310	233.1 \pm 17.5	12444	638.3 \pm 26.5
MS0317.0+1834	0.19	15/01/97	4359	293.9 \pm 19.0	14976	1905.3 \pm 45.1
1ES0347-121	0.188	10/01/97	6492	577.0 \pm 26.9	10675	1254.9 \pm 36.6
1ES0414+009	0.287	21-22/09/96	—	—	11039	1858.4 \pm 44.1
1ES0502+675	—	6-7/10/96	—	—	11045	4117.3 \pm 64.9
MS0737.9+7441	0.315	29-30/10/96	3075	37.1 \pm 7.8 ^a	23279	735.9 \pm 30.6
1ES1101-232	0.186	4/01/97	5195	2484.2 \pm 51.1	13830	9509.3 \pm 98.1
1ES1133+704 (Mkn 180)	0.046	10-11/12/96	4078	439.2 \pm 22.6	18266	1940.7 \pm 45.8
MS1312.1-4221	0.108	21/12/97	3541	228.2 \pm 17.5	5555	446.7 \pm 22.0
1ES1517+656	—	5/03/97	4536	779.3 \pm 29.5	11130	2273.3 \pm 48.6

^a counts from a 3/4 of a circle, excluding the bottom-right quadrant that contains a non-related source.

For this reason we have scrutinized all sources for variability over time scales of 500 or 1000 seconds, so as to have about ten different bins in the course of the observation. No variability is observed during each observation (a fit with a constant is always acceptable). Therefore we will analyze each dataset as a whole to derive spectral information (see Section 3.2).

On time scales longer than the *BeppoSAX* pointing, variability is inferred from comparison with other observations (see e.g., below in Section 6, and Figure 4). Most of the sources have been observed with ROSAT in an energy band very close to the *BeppoSAX* low energy band. We will therefore present the ROSAT data and a comparison with the *BeppoSAX* ones in Section 4.

3.2. Spectral Analysis

The three MECS units spectra have been summed together to increase the S/N, after having checked that fits on separate spectra yielded consistent results within the statistical uncertainties.

All sources appear pointlike in both the LECS and MECS images. Counts are extracted in a circular region of 8.5'/4' (LECS/MECS) radius whenever possible¹. This region contains at least 95% of the photons from the source.

The background is taken from the distributed blank sky images, in a region corresponding to the one used to extract source counts. The variability of the MECS background across the field of view due to vignetting, strongback obscuration and the spilling of 5.9 keV calibration source photons is not known yet with high accuracy. Given that this variability effect is higher than the secular modulation of the total instrumental+cosmic background, which has been estimated to be $\simeq 30\%$, blank fields background has been favored over an estimate from the same image in a different, albeit close, location. Since the back-

¹ i.e., when there is no other source in the 8.5'/4' radius; this is the case for all sources except MS0737.9+7441, in which counts are extracted from a region corresponding to a circle from which the bottom right quadrant is excluded.

ground flux is never higher than 10% of the source's flux, the secular modulation has a negligible effect on the spectral results.

Extraction of the data is done in FTOOLS v4.0 and counts are binned so as to have at least 30 total counts in each bin to ensure applicability of the χ^2 statistics; the spectral analysis is performed in XSPEC v.9.0 (Shafer et al. 1991), using the matrices produced in September 97 that include the most recent updates in calibrations. Net counts and errors for each source are listed in Table 1.

We fitted together LECS and MECS, leaving free the LECS normalization with respect to the MECS normalization to account for the residual errors in intensity cross-calibration (see Cusumano, Mineo, Massaro et al. 1998, in preparation); the assumed spectral shape is a single power-law model plus free low energy absorption, arising from cold material with solar abundances (Morrison and McCammon, 1983). When no LECS data are available, only the MECS data are fitted; in this latter case the N_{H} value is fixed to the Galactic one, since the energy range of the MECS does not allow a firm determination of the absorbing column. Fits to the LECS data are performed only up to 4 keV, as the response matrix of LECS is not well calibrated above this energy (see Orr et al. 1998).

The parameters of the best fit with free N_{H} and single power law are given in Table 2 for all sources. Galactic N_{H} values, as derived from the 21 cm radio survey by Dickey and Lockman (1990) (or by the pointed observation by Elvis et al. 1989 when available) at the position of the source, are listed for reference. Errors on the fitted parameters are given with 90% confidence for one interesting parameter ($\Delta\chi^2 = 2.706$). Unabsorbed fluxes (i.e., corrected for Galactic absorption) derived from the fit are given in the 2-10 keV band. We give also the best fit value for the normalization factor of the LECS relative to MECS. The values fall in the range expected given the current knowledge of the cross-calibration (F. Fiore, private communication; see also http://www.sdc.asi.it/software/cookbook/cross_cal.html).

All the objects except 1ES1101-232 are well fitted by a power law with low energy absorption at a confidence

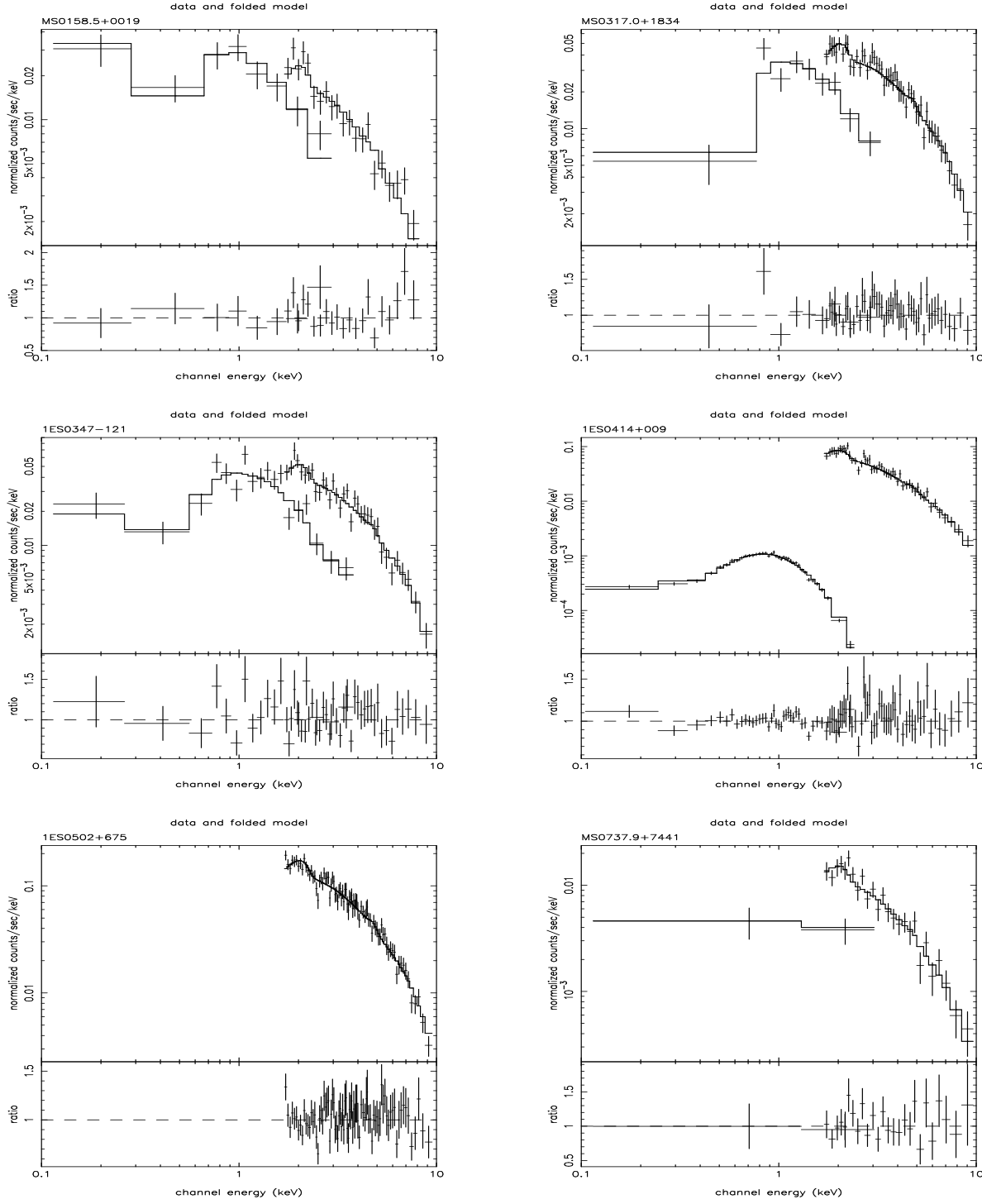


Fig. 1. a X-ray (LECS and MECS) data and fitted spectrum (from Table 3 or Table 2), and ratio of data to fit. MS0158.5+0019, MS0317.0+1834, 1ES0347-121, 1ES0414+009 (no LECS data, includes also ROSAT/PSPC data; note that ROSAT data are in $\text{counts sec}^{-1} \text{ keV}^{-1} \text{ cm}^{-2}$), 1ES0502+675 (no LECS data), MS0737.9+7441.

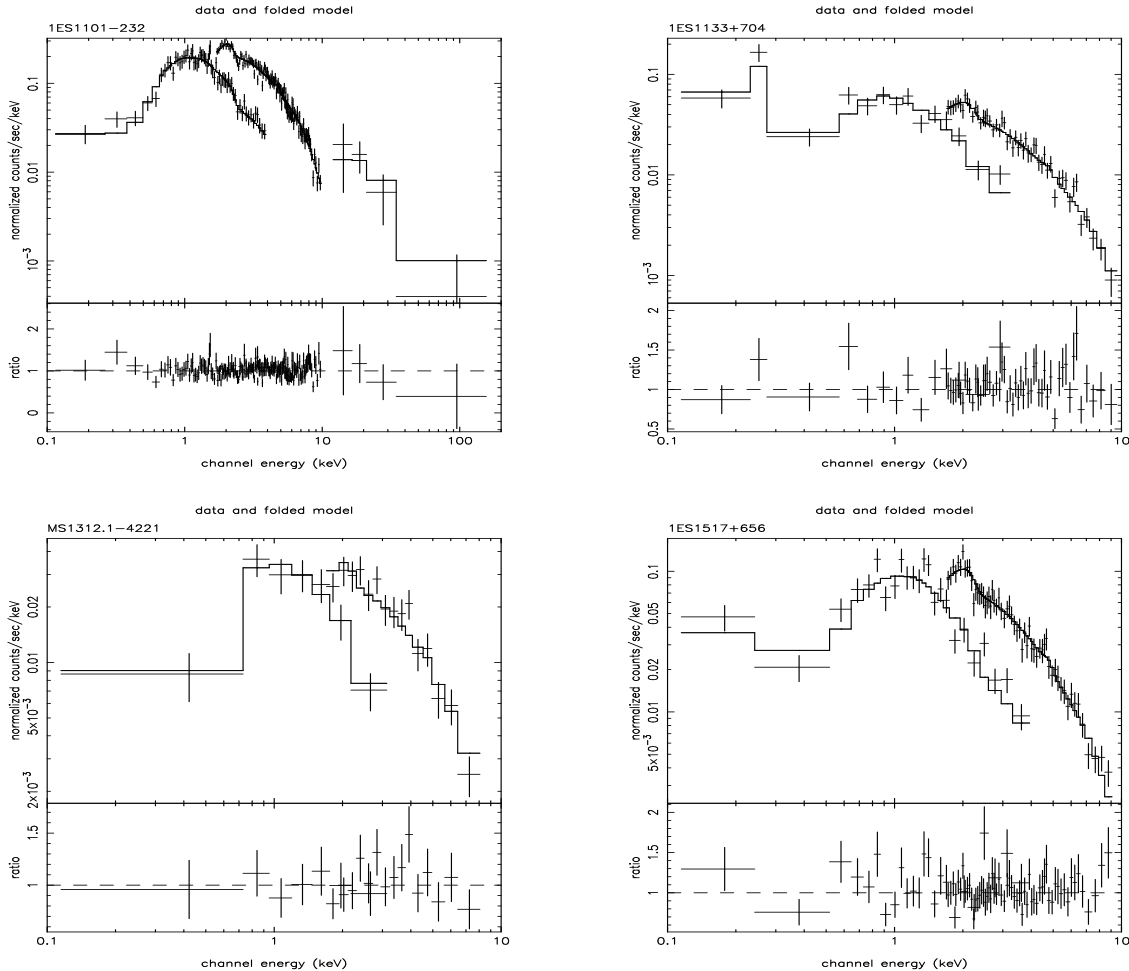


Fig. 1. b (Continued) X-ray (LECS and MECS) data and fitted spectrum (from Table 3 or Table 2), and ratio of data to fit. 1ES1101-232 (includes also PDS data), 1ES1133+704, MS1312.1-4221, 1ES1517+656.

level $\geq 90\%$; the slopes range between 1 and 1.5, with a roughly flat distribution of occurrences and an average $\langle \alpha_x \rangle = 1.31 \pm 0.06$. In two cases (1ES1133+704 and 1ES1517+656) the fitted N_{H} is higher than the Galactic value by more than a factor of two (at 2.9 and 3.4σ , respectively). This might indicate an intrinsic absorption, a more complex spectrum like a broken power law, or other features at low energy. Furthermore, residuals are skewed at high energies in MS0158.5+0019, and at low energies in 1ES0347-121, 1ES1101-232 and 1ES1517+656, even when the fit is formally acceptable. This could be attributed to low energy absorption edges or changes of slope, although a residual contamination in the calibration of the matrix at the present status is still possible (at the $\sim 15\%$ level in the 0.4-0.5 keV interval, Orr et al., 1998).

To better understand the situation we have tried, for the eight objects for which we have the LECS data, a more complex model for the fit, under the assumption that the

low energy absorption is not intrinsic to the object but only due to the intervening (Galactic) material. We therefore use a broken power law with low energy absorption fixed to the Galactic value (as in Table 2) and α_1 , α_2 (the energy indices describing the power law spectral shape below and above the break energy E_0) and E_0 free to vary. We fix also the LECS/MECS normalization to the values found in Table 2. In six out of eight cases an improvement (F-test probability $\geq 99\%$) is found over the case of fixed Galactic N_{H} and single power law. In the other two cases either the broken power law reduces to a single one ($\alpha_1 = \alpha_2$; MS0158.5+001), or the improvement has a marginal probability (58%) and the parameters are poorly constrained (MS1312.1-422).

Results of the six fits at $P \geq 99\%$ in the broken power law case are listed in Table 3, together with the χ^2_{ν} value and its probability. The derived probabilities are roughly equal or better than the corresponding probabilities found

Table 2. Fit results for a single power law spectrum and free N_{H}

Name	Energy Index	$N_{\text{H}}^{\text{Gal}}$ $\times 10^{20} \text{ cm}^{-2}$	N_{H} $\times 10^{20} \text{ cm}^{-2}$	$F_{\text{MECS}}^{\text{a}}$ (2-10)keV	$F_{1\text{keV}}$ μJy	Norm. (LECS/MECS)	χ_{ν}^2 (dof)	Prob.
MS0158.5+0019	$1.27^{+0.18}_{-0.18}$	2.67	$2.9^{+1.3}_{-1.0}$	2.61	1.03	0.89	0.99 (25)	45%
MS0317.0+1834	$1.08^{+0.11}_{-0.10}$	10.5	$22.0^{+13.0}_{-9.3}^e$	6.94	2.05	0.72	0.73 (56)	95%
1ES0347-121	$1.17^{+0.11}_{-0.10}$	3.64	$4.7^{+2.0}_{-1.1}$	6.19	2.05	0.71	1.17 (49)	20%
1ES0414+009	$1.54^{+0.10}_{-0.10}$	9.15 ^b	— ^c	8.25	5.22	—	0.82 (45)	80%
1ES0502+675	$1.34^{+0.06}_{-0.06}$	9.27	— ^c	19.05	8.51	—	1.00 (79)	50%
MS0737.9+7441 ^d	$1.53^{+0.28}_{-0.23}$	3.54	$25.8^{+49.3}_{-21.6}^e$	1.54	0.88	0.68	0.81 (24)	72%
1ES1101-232	$1.03^{+0.05}_{-0.04}$	5.76	$8.9^{+3.7}_{-1.7}$	37.92	10.23	0.70	1.13(181)	10%
1ES1133+704	$1.47^{+0.09}_{-0.09}$	1.27 ^b	$3.0^{+0.8}_{-0.6}^f$	5.10	2.61	0.68	1.01 (62)	48%
MS1312.1-4221	$1.21^{+0.20}_{-0.19}$	8.19	$11.7^{+11.5}_{-5.6}$	4.26	1.52	0.85	0.74 (18)	75%
1ES1517+656	$1.44^{+0.09}_{-0.09}$	2.12	$7.6^{+3.2}_{-1.6}^f$	10.27	4.99	0.68	1.18 (79)	15%

^a Unabsorbed flux in $10^{-12} \text{ erg cm}^{-2} \text{ s}^{-1}$

^b From Elvis et al. 1989

^c Fixed N_{H}

^d MS0737.9+7441: There are other sources nearby. LECS count are therefore extracted from an area 3/4 of a circle, excluding the other sources; the normalization has been corrected multiplying by 4/3. The effect on the slope is minimal.

^e marginally consistent with Galactic N_{H} (at $\leq 2\sigma$)

^f not consistent with Galactic N_{H} (at $\sim 3\sigma$)

in Table 2 (note that the number of free parameters in Table 2 is the same as in Table 3 since also the normalization LECS/MECS was left free). This implies that the broken power law with Galactic absorption is a good representation of the observed spectra, from a statistical point of view.

A good determination of the confidence interval (90% level for one interesting parameter) for all the parameters is possible only for the two sources with higher statistics, however the α_2 values are generally well constrained and consistent with the slope of the single power law fit, while the $\Delta\alpha$ is on average about 0.5, consistent with other results for BL Lacs (e.g., Sambruna et al. 1996; Urry et al. 1996). Therefore, the hypothesis that the apparent excess in absorption could instead be due to an intrinsically curved (convex) spectrum seems to be plausible.

The brightest source of the sample (1ES1101-232) has been detected (at 3.5σ) also in the PDS in just $\sim 6\text{k}$ s of on-source observing time. We have therefore a measurement at the same epoch of the spectrum between 0.1 and ~ 100 keV (see spectrum in Figure 1). Net on-source PDS spectra have been obtained simply subtracting “off-” from “on-position” ones. The spectra of the four units have then been summed together after energy equalization. Very short ($\tau < 1$ s) and intense spikes, due to single-particle-induced fluorescence in the crystals, have been removed applying the method described in Matt et al. (1997). We fitted the PDS spectrum together with LECS and MECS spectra: the slope is flat and consistent with the same slope as the MECS above ~ 1.5 keV (see α_2 value from Table 3). This results imply that the harder energy band is within reach with exposures of some tens

of ksec for many objects of the sample, especially those with a flat spectrum.

Spectra for the 10 sources are shown in Figure 1, including the best fit model derived from the broken power law model for the six sources of Table 3, and from the single power law model for the other four sources, and including the PDS data for 1ES1101-232, and the ROSAT/PSPC data for 1ES0414+009 (see Section 4).

We have also computed the upper limits in the PDS, under the assumption that the spectral slope derived in the MECS continues into the PDS band, and plotted the results in the overall spectra presented in Figure 4 (see Section 6). No source was detected in the HPGSPC, which has a better energy resolution but lower effective area than the PDS.

4. Comparison with ROSAT Observations

4.1. Data and spectral Analysis

Eight out of ten sources have been observed by the PSPC instrument onboard ROSAT and some of them have been previously published by different authors (the EMSS sources, Perlman et al. 1996b). In order to ensure a uniform procedure for all the sample we have re-analyzed them, obtaining results consistent with those published. We have processed the data with a standard reduction procedure, as described e.g. in Comastri Molendi & Ghisellini (1995).

All the 8 sources have been clearly detected with enough counts to allow spectral analysis. The background-subtracted light curves are not variable over the entire observation, typically lasting 3–9 ksec with maximum deviations of the order of 30–40 %, likely due entirely to

Table 3. Fit results for a broken power law spectrum

Name	Energy Index(α_1)	Energy Index(α_2)	E_0 keV	F_{MECS}^a (2-10)keV	χ^2_ν (dof)	Prob.
MS0317.0+1834	0.39 uncertain	1.01(0.93-1.10)	0.93 uncertain	6.90	0.75(56)	92%
1ES0347-121	0.87(0.78-1.08)	1.23(1.13-1.33)	1.45 uncertain	6.10	1.10(49)	29%
MS0737.9+7441	0.17 uncertain	1.43(1.27-1.61)	1.18(0.6 - 3.)	1.51	0.82(24)	71%
1ES1101-232	0.59(0.35-0.74)	1.05(1.01-1.08)	1.36(1.11-1.65)	37.63	1.06(181)	28%
1ES1133+704	0.85(<1.13)	1.47(1.39-1.57)	0.93(<2.13)	5.08	1.01(62)	45%
1ES1517+656	0.40(0.15-0.59)	1.48(1.41-1.56)	1.25(1.08-1.43)	10.09	1.02(79)	43%

^a Unabsorbed flux in 10^{-12} erg cm $^{-2}$ s $^{-1}$

Table 4. Fits in the 0.1–2 keV energy range, using ROSAT data.

Name	N_H $\times 10^{20}$ cm $^{-2}$	F_1^a keV μJy	α_{ROSAT}	χ^2_ν (d.o.f.)	N_{HGal} $\times 10^{20}$ cm $^{-2}$	α_{ROSAT}	χ^2_ν (d.o.f.)
MS0158.5+0019	3.0(2.3–3.6)	1.34	1.45(1.23–1.68)	0.63 (14)	2.67	1.35(1.28–1.43)	0.63 (15)
MS0317.0+1834	9.5(6.7–14.1)	0.56	1.50(1.02–2.04)	1.81 (13)	10.5	1.63(1.32–1.91)	1.70 (14)
1ES0347–121	3.6(3.3–3.8)	2.55	1.10(1.02–1.19)	1.01 (42)	3.64	1.13(1.09–1.16)	1.00 (43)
1ES0414+009	9.5(9.1–10.0)	4.69	1.63(1.56–1.71)	1.20 (36)	9.15	1.58(1.54–1.62)	1.22 (37)
MS0737.9+7441	4.1(3.8–4.5)	1.73	1.34(1.23–1.45)	1.38 (37)	3.54	1.16(1.13–1.20)	1.54 (38)
1ES1101–232	6.8(6.4–7.1)	11.2	1.43(1.35–1.51)	1.08 (35)	5.76	1.23(1.20–1.27)	1.67 (36)
1ES1133+704	1.3(1.1–1.6)	2.60	1.31(1.22–1.40)	1.94 (32)	1.27	1.29(1.26–1.32)	1.89 (33)
1ES1517+656	3.6(3.3–3.9)	7.42	1.29(1.19–1.39)	1.14 (49)	2.12	0.82(0.78–0.85)	2.49 (50)

^a Model flux at 1 keV.

instrumental effects. In principle however variations on time scales of the order of ~ 0.5 ksec were accessible. The source spectra were rebinned in order to obtain a significant S/N (> 5) for each bin and fitted with a single power-law model plus absorption arising from cold material with solar abundances (Morrison & McCammon 1983). The derived spectral parameters are given in Table 4, where the reported errors are at 90% confidence level for one interesting parameter. All the spectra were fitted with the column density i) fixed at the Galactic value, and ii) free to vary. Values for the Galactic column densities towards the objects in our sample are reported for ease of reference from Table 2.

In most cases a single power law spectrum with the absorption fixed at the Galactic value provides an excellent description of the data, while for some of the objects either the fits are statistically unacceptable and/or the column density inferred from the fit is not consistent with the Galactic value, thus requiring a more complex description of the spectral shape.

4.2. Comparison between BeppoSAX and ROSAT Results

We compare the *BeppoSAX* and ROSAT data as taken from Table 2 and Table 4, respectively. We plot the two fluxes at 1 keV in Figure 2, assuming total errors to be 10% of the flux (higher than those from counting statistics only and taking into account residual absolute calibrations); the solid line represents the $F_{MECS} = F_{PSPC}$ locus. From the comparison of the ROSAT and *BeppoSAX*

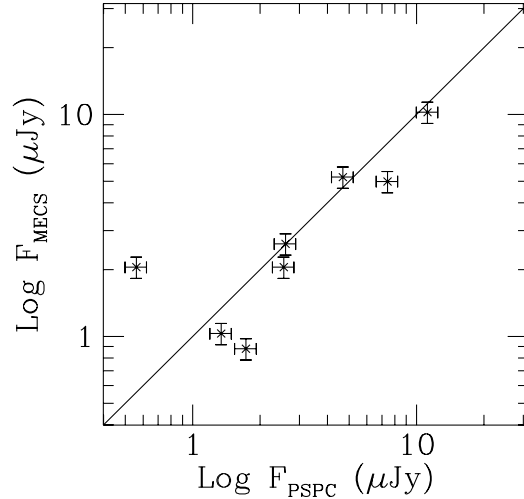


Fig. 2. X-ray flux at 1 keV from *BeppoSAX* vs. X-ray flux at 1 keV from ROSAT in μJy. Errors are 10% of the flux. The solid line represents the locus of $F_{MECS} = F_{PSPC}$.

results it emerges that, although these observations cover a time interval of few years, the 1 keV fluxes of the various sources are practically the same within 30% for all but three sources: MS0317.0+1834, with a *BeppoSAX* flux

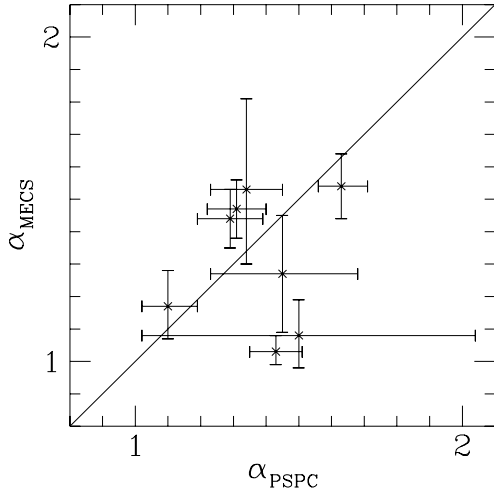


Fig. 3. α_x from *BeppoSAX* vs. α_{PSPC} from ROSAT. The solid line represents the locus of $\alpha_x = \alpha_{PSPC}$.

$\sim 4 \times$ larger, and MS0737.9+7441, and 1ES1517+656 with a ROSAT flux ~ 2 and $\sim 1.5 \times$ larger, respectively.

The ROSAT and *BeppoSAX* single power law spectral indices, plotted one against the other in Figure 3, are also consistent for all but one source: 1ES1101-232; in particular the PSPC spectrum of this source can be fitted also by a broken power law, with N_{H} fixed at the Galactic value² but the values of the parameters are inconsistent with those found in the *BeppoSAX* observation. This may be an indication that, even if the source flux is roughly the same, in 1ES1101-232 there has been a variation of the spectrum and in particular of the position of the peak of the synchrotron emission.

Instead, with respect to the N_{H} values as determined with the two satellites, the situation is more complex. First of all, the ROSAT values are probably more reliable than the *BeppoSAX* ones, given the small number of counts usually detected in the LECS for our sources (only for 1ES1101-232 we have good statistics in the LECS). The ROSAT N_{H} values are consistent with the Galactic ones for five sources out of eight while for the other three (MS0737.9+7441, 1ES1101-232 and 1ES1517+656) the F-test shows that introducing N_{H} as a free parameters improves the χ^2 significantly (97.4%, 99.99%, and $>99.99\%$, respectively). For MS0158.5+0019 and 1ES0347-121 the N_{H} measured by the PSPC is also consistent with that measured from the LECS/MECS data. In the other cases

² Results of the fit: $\alpha_1 = 1.07$ (0.85 - 1.16); $\alpha_2 = 1.42$ (1.33 - 1.54); $E_0 = 0.69$ (0.44-0.93) keV with a $\chi^2 = 42.3$ (33 dof) and an F-test probability with respect to the fixed Galactic N_{H} and single power law of 99.99%.

the PSPC sees a lower amount of N_{H} (and with smaller error intervals) than the LECS/MECS data.

Again these are clear indications in favor of a more complex spectrum than a simple power law (see section 3.2). Indeed, a broken power law with N_{H} fixed to the Galactic value seems a better representation to the *BeppoSAX* data for all these five sources (see Table 3).

For 1ES0414+009, for which the intensities in the MECS and PSPC are comparable, and for which we lack a determination of the low energy portion of the spectrum (no LECS data), we combine the two instruments, PSPC and MECS for a simultaneous fit (see Figure 1). The slope is $\alpha = 1.59 \pm 0.6$, consistent with α_x from the MECS only, and $N_{\text{H}} = 9.3 \pm 0.4 \times 10^{20} \text{ cm}^{-2}$, consistent with the Galactic value.

5. Same-Epoch Optical Observations

In the course of an optical observing campaign performed at the Torino Observatory, the eight sources with declination greater than -20° were observed during or close to the time of *BeppoSAX* pointing. The data were taken with the 1.05 meter REOSC telescope. The equipment includes a 1242×1152 pixel CCD detector with a 0.47 arcsec per pixel scale and standard Johnson's *BV* and Cousins' *R* filters.

Data reduction was obtained with the Robin procedure developed at the Torino Astronomical Observatory (Villata et al. 1997), which performs bias subtraction, flat field correction, and circular Gaussian fit after background subtraction.

Magnitude calibration was derived through comparison with reference stars in the same field of the source; for MS0158.5+0019 and MS0317.0+1834 we used the photometric sequences published by Smith et al. (1991), while for the other BL Lacs we adopted our own sequences: those in the field of 1ES0502+675, MS 0737.9+7441, 1ES1133+704, and 1ES1517+656 are published in Villata et al. (1998).

Optical light curves of the eight BL Lacs in the period around the *BeppoSAX* pointings are shown in Raiteri et al. (1998). Table 5 gives the data closest in time to the SAX observations.

Using the same epoch optical magnitudes for the 8 objects north of -20° , and literature magnitudes for 1ES1101-232 and MS1312.1-4221, we compute the two point spectral indices α_{ox} and α_{ro} , reported in Table 6 together with α_{rx} , $\log(F_x/F_r)$ and L_x , and ν_{peak} computed in the next Section. The frequencies used to compute the broad band indices are 5 GHz, 2500 Å and 2 keV. We apply a K-correction using $z = 0.2$ for the two sources with unknown redshift, $\alpha_r = 0.2$, $\alpha_o = 0.65$ and α_x from Table 2.

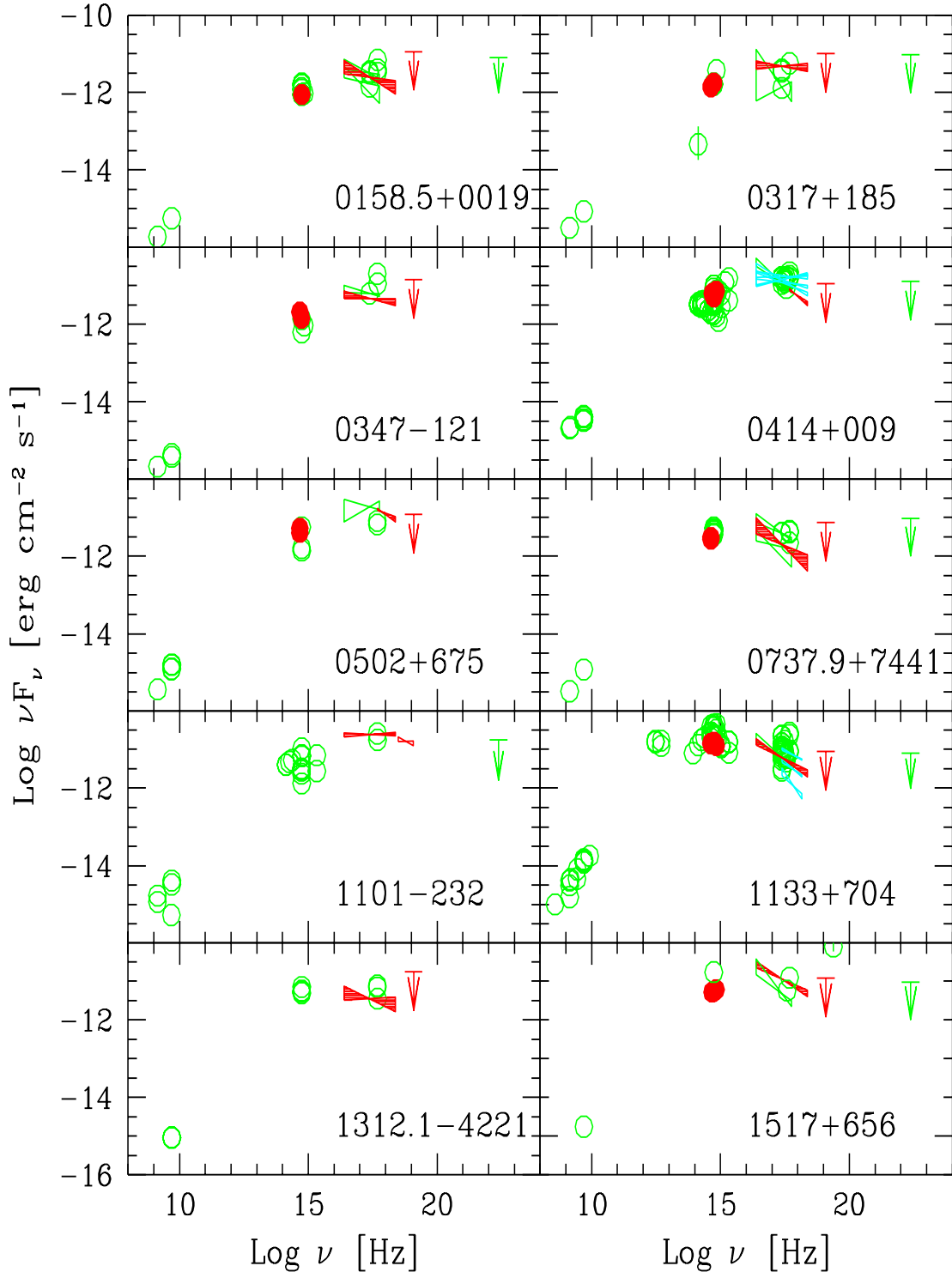


Fig. 4. The spectral energy distribution of the XBLs. Data from *BeppoSAX* spectra and same epoch optical magnitudes from this paper are in filled symbols, data from literature (open symbols or upper limits) are referenced in Table 7. The name of the object is indicated in each panel.

Table 5. Same-epoch Optical Magnitudes

SOURCE	BeppoSAX date	OPTICAL date	R	V	B
MS0158.5+0019	16-17 Aug 96	22 Oct 96		18.60±.10	
		31 Oct 96	>17.7		
MS0317.0+1834	15 Jan 97	18 Dec 96	18.10±.08		
		16 Jan 97	17.83±.08		
		16 Jan 97		18.33±.10	
		29 Jan 97	18.02±.08		
1ES0347-121	10 Jan 97	17 Dec 96	17.38±.08		
		10 Jan 97	17.37±.08		
		13 Jan 97	17.33±.08		
		13 Jan 97		18.10±.10	
1ES0414+009	21-22 Sep 96	19 Oct 96		16.86±.04	
		23 Oct 96		16.86±.04	
1ES0502+675	06-07 Oct 96	18 Oct 96		17.30±.04	
		23 Oct 96		17.01±.04	
MS0737.9+7441	29-30 Oct 96	07 Nov 96	17.44±.08		
		27 Nov 96	17.29±.08		
1ES1133+704	10-11 Dec 96	18 Dec 96	14.85±.04		
		14 Jan 97	14.94±.04		
		14 Jan 97		15.38±.04	
		14 Jan 97			16.04±.13
1ES1517+656	05 Mar 97	02 Mar 97	16.11±.03		
		05 Mar 97	16.11±.03		
		06 Mar 97	16.08±.03		
		10 Mar 97	16.08±.03		
		13 Mar 97	16.08±.03		
		13 Mar 97		16.43±.03	
		13 Mar 97			16.78±.05

Table 6. Derived quantities: Two-point overall spectral indices (α_{ox} ; α_{ro} ; α_{rx}), X-ray-to-radio flux ratio, logarithm of X-ray luminosity, and logarithm of ν_{peak} .

Name	α_{ox}	α_{ro}	α_{rx}	$\log(F_x/F_r)$	$\log L_x$	$\log \nu_{peak}$
MS0158.5+0019	0.89	0.44	0.59	-9.71	45.12	16.73
MS0317.0+1834	0.78	0.44	0.55	-9.39	45.11	17.01
1ES0347-121	0.83	0.37	0.52	-9.16	45.05	16.97
1ES0414+009	0.95	0.49	0.64	-10.16	45.59	16.47
1ES0502+675	0.76	0.42	0.53	-9.24	45.6 ^a	16.83
MS0737.9+7441	1.09	0.43	0.64	-10.19	44.93	15.97
1ES1101-232	0.76	0.47	0.57	-9.50	45.83	17.48
1ES1133+704	1.29	0.44	0.71	-10.64	43.69	15.65
MS1312.1-4221	1.12	0.32	0.58	-9.63	44.85	15.90
1ES1517+656	0.99	0.37	0.57	-9.56	45.3 ^a	16.60

^a Redshift unknown; z=0.2 assumed to compute luminosity

6. Spectral Energy Distributions

In Fig. 4 we plot the spectral energy distribution (SED) of our sources, reporting the *BeppoSAX* spectral fits and the nearly simultaneous optical data when available (filled symbols), and other data from the literature (open symbols or lower limits; references are listed in Table 7).

As can be seen, the SED of the objects in our sample are characterized by a smooth distribution, rising (in νF_ν) from the radio to the optical-UV and X-ray bands. Variability is evident, especially in the most often observed

objects. Many objects show a fall off at high energies. In order to obtain a reliable estimate of the peak energy, the SED of each object has been fitted with a polynomial function of the type

$$\log(\nu F_\nu) = a + b(\log \nu) + c(\log \nu)^2 + d(\log \nu)^3 \quad (1)$$

(see Comastri et al. 1995). For the fit, we adopted the *BeppoSAX* data for the X-ray band, and same-epoch optical data when available. For the other bands (i.e., radio and IR – none of these sources has been detected in γ -rays) we

Table 7. References for data shown in Fig. 4

MS0158.5+0019	G95, J94, L96, P96a, P96b, N96, W94	
MS0317.0+1834	G93, G95, L96	
1ES0347-121	G95, L96, P96a	
1ES0414+009	B92, F93, G95, GC91, Gr95, IT88, L96, M90, P96a, Pi94, Pi93, Sa94	
1ES0502+675	B94, B95, G95, GC91, P96a	
MS0737.9+7441	G95, J94, L96, P96a, PS93, W94	References: B92: Bersanelli et al.,
1ES1101-232	B92, E92, F93, F94, G95, L95, P94, P96a, Pi93, R89	
1ES1133+704	B95, Bi92, C95, E92, G90, G95, GS95, IN88, K91, L96, MB86, N96, P92, P96a, PG95, Pi93, Sa94, T84, WW90	
MS1312.1-4221	G95, P96a, S90	
1ES1517+656	B94, G95, MB95, P96a	

1992; B94: Brinkmann et al., 1994; B95: Brinkmann et al., 1995; Bi92: Biermann et al., 1992; C95: Ciliegi et al., 1995; E92: Edelson et al., 1992; F93: Falomo et al., 1993; F94: Falomo et al., 1994; G90: Giommi et al., 1990; G93: Gear, 1993; G95: Giommi et al., 1995; GC91: Gregory & Condon, 1991; Gr95: Griffith et al., 1995; GS95: Ghosh & Soundararajperumal, 1995; IN88: Impey & Neugebauer, 1988; IT88: Impey & Tapia, 1988; J94: Jannuzzi et al., 1993; K91: Kinney et al., 1991; L95: Lanzetta et al., 1995; L96: Lamer et al., 1996; M90: Mead et al., 1990; MB86: Mazzarella & Balzano, 1986; MB95: McNaron-Brown et al., 1995; N96: Nass et al., 1996; P92: Patnaik et al., 1992; P94: Pesce et al., 1994; P96a: Perlman et al., 1996a; P96b: Perlman et al., 1996b; PG95: Padovani & Giommi, 1995; Pi93: Pian & Treves, 1993; Pi94: Pian et al., 1994; PS93: Perlman & Stocke, 1993; R89: Remillard et al., 1989; S90: Stocke et al., 1990; Sa94: Sambruna et al., 1994; T84: Tovmassian et al., 1984; W94: Wolter et al., 1994; WW90: Worrall & Wilkes, 1990.

used the maximum observed value: variability amplitudes are not large in these bands and so should not affect significantly the results. From the fitted polynomial we derive the peak frequency of the SED ν_{peak} .

Three of the sources in this sample have been studied also by Sambruna et al. (1996), where the ν_{peak} value was derived assuming a parabolic fit. If we compare the ν_{peak} values derived here and in Sambruna et al. (1996), in two cases (MS0158.5+0019 and MS0737.9+7441) we have consistent results, while in the third (MS0317.0+1834) ν_{peak} differs by about 2.5 orders of magnitudes ($\log \nu_{peak} = 17.01$ vs. $\log \nu_{peak} = 14.36$ in Sambruna et al. 1996). Note, however, that their Figure 4 shows that the peak of the emission for MS0317.0+1834 is indeed at higher energies, in agreement with our value. Note also that the optical simultaneous observations constrain ν_{peak} in a much better way.

Figure 5 shows the spectral indices derived from the LECS/MECS fit (from Table 2) vs. $\log \nu_{peak}$. We include also the data for the objects studied by Comastri et al. (1995), which are 9 LBL (crosses) and 3 HBL (empty circles). These latter points are derived from ROSAT observation and so sample the spectra at slightly lower energy. A program is underway to observe a sample of BL Lacs extracted from the 1 Jy sample (Padovani et al. 1998 and in preparation). When a sizable sample of LBL will be observed by *BeppoSAX*, a more direct comparison will be possible. For the HBL objects there is a good anti-correlation between α_x and ν_{peak} (correlation probability = 95%). The solid line represents the linear regression ob-

tained with the 10 objects observed by *BeppoSAX* using the OLS bisector method (Isobe et al. 1990). The same-epoch data used for most sources, that remove the uncertainty due to variation for the determination of ν_{peak} , are important in order to obtain such a tight correlation. The LBL are less correlated (correlation probability $\sim 80\%$).

The behavior of α_x with ν_{peak} , illustrated in Figure 5, reflects the large range of frequencies at which the synchrotron peak is observed to lie. This picture is consistent with the one proposed by Padovani and Giommi (1996) using ROSAT data, in which HBL are characterized by a synchrotron peak located in the EUV/X-ray band: the X-ray radiation is therefore produced by the synchrotron process. According to the exact location of ν_{peak} , the X-ray spectrum changes, being flat ($\alpha_x \leq 1$) in extreme HBL objects (where ν_{peak} lies in the X-ray band), and steeper as the peak migrates to the UV band. In LBL objects ν_{peak} has moved in the optical-IR band and the X-ray band is dominated by the flat inverse Compton spectrum.

In Figure 6 we plot for both these ten HBL with *BeppoSAX* data and the Comastri et al. (1995) objects the relationship between α_{rx} and $\log \nu_{peak}$. We add the linear regression obtained using the OLS bisector method with the *BeppoSAX* data only (solid line) and extrapolated down to the LBL region (dotted line), besides the constant α_{rx} (horizontal dashed line) derived following Padovani & Giommi (1995) (see their Figure 12). The HBL points are correlated at the 98% level, indicating a link between the two quantities, while the LBL points are consistent both with the extrapolation of the regression, or with the

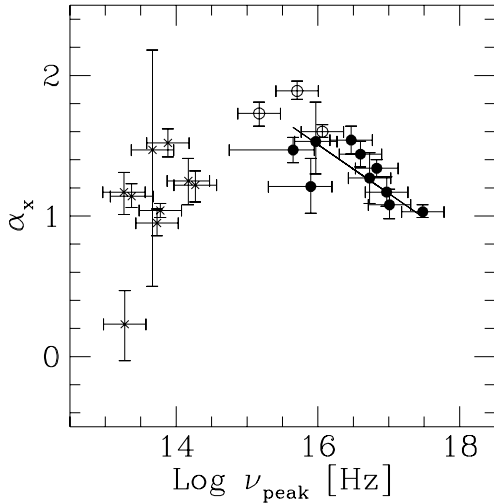


Fig. 5. α_x as a function of ν_{peak} . Filled circles are HBL with α_x values from *BeppoSAX* as in Table 2, ν_{peak} from fit of SED – see Section 6. Empty circles (HBL) and crosses (LBL) are from Comastri et al. (1995) in which α_x is derived from ROSAT observations. The solid line represent the linear regression (with the OLS method) between the 10 HBL observed by *BeppoSAX*.

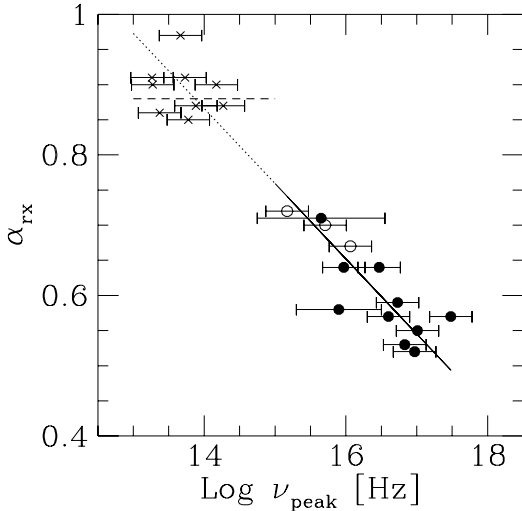


Fig. 6. α_{rx} as a function of ν_{peak} . Filled circles are HBL: α_{rx} values from Table 6, ν_{peak} from fit of SED – see Section 6. Empty circles (HBL) and crosses (LBL) are from Comastri et al. (1995) in which α_x is derived from ROSAT observations. The solid line represents the linear regression fit using the OLS method on the 10 objects observed by *BeppoSAX* while the dotted line indicates its extrapolation to lower values of ν_{peak} . The horizontal dashed line ($\alpha_{rx} = \text{constant}$) is derived from the model described in Padovani & Giommi 1995 for LBL objects.

constant value for α_{rx} suggested by Padovani & Giommi (1995), in the hypothesis that for LBL the X-ray flux is proportional to the radio flux.

Again, it will be indeed interesting to compare these results with those obtained for LBL with *BeppoSAX* data (Padovani et al., in preparation).

7. Results and Conclusions

We have analyzed the spectra for 10 X-ray selected BL Lacs observed with the Narrow Field Instruments on board the *BeppoSAX* satellite.

The sources are detected from ~ 0.2 up to ~ 10 keV (and in one case up to ~ 100 keV with the PDS instrument) with a very smooth appearance. The spectrum is generally well fitted by either a single power law, or by a broken convex power law that most probably represents the steepening after the synchrotron peak, whose position is determined also by using simultaneous optical observations.

Variability is not present during the short *BeppoSAX* exposure; analysis of ROSAT data shows for most of the sources little variability (within $\sim 30\%$) with respect to the *BeppoSAX* flux and spectral indices consistent with the *BeppoSAX* ones. The spectral energy distributions, which include literature data, instead show variability in all bands.

The X-ray spectral indices α_x range between 1 and 1.5 with a flat distribution and a mean value $\langle \alpha_x \rangle = 1.31 \pm 0.06$. The scatter in the distribution is due to an anti-correlation we have found between α_x and the frequency of the peak of the emission, ν_{peak} . This extends to the *BeppoSAX* band a correlation which had been discovered in the ROSAT band for this class of objects. The fact that sources with harder X-ray spectra have higher ν_{peak} is expected if the *BeppoSAX* band is still dominated by synchrotron emission, which is also consistent with the spectral energy distributions of our BL Lacs.

Furthermore, we have no evidence of a spectral flattening (indicating the arising of the Compton component) in the present spectra, but future PDS detections, that are possible with exposure times slightly longer than those obtained here, might help in this respect.

The large fraction (at least 2 out of 10) of HBL selected in the soft X-ray band found with a flat ($\alpha_x \sim 1$) X-ray slope (i.e., they are near the peak of the synchrotron emission) and the distribution of α_x values support the view that objects with even higher spectral peaks in their quiescent status indeed exist, and might be found in large numbers if we devise the correct strategy (e.g., samples at harder X-rays, TeV sources, etc.)

Moreover, these sources are good candidates to be TeV emitters. In fact, in the sources with the flattest α_x the peak of the synchrotron component is localized in the soft X-ray range. Electrons emitting at 1 keV by the synchrotron process have Lorentz factors

$\gamma \sim 2.5 \times 10^5 (\nu_{peak,1 \text{ keV}}/B\delta)^{1/2}$, where $\nu_{peak} = 2.42 \times 10^{17} \nu_{peak,1 \text{ keV}} \text{ Hz}$, B is the value of the magnetic field in Gauss and δ is the usual Doppler factor. Through the inverse Compton mechanism, they can emit up to $E \sim \gamma m_e c^2 \delta \sim 130 (\nu_{peak,1 \text{ keV}} \delta / B)^{1/2} \text{ GeV}$. If the magnetic and radiation energy densities are equal (as it is, approximately, in the three BL Lacs already detected in the TeV band), the flux level of the synchrotron and inverse Compton peaks is roughly equal. Low redshift sources are therefore good candidates to be *detected* in the GeV–TeV band, while the high energy emission of the more distant sources could be absorbed in $\gamma\gamma$ interactions with the background IR photon field, whose intensity is still uncertain. Indeed, a cutoff in the high energy spectrum could be used to determine the IR background (see, e.g. Stecker & De Jager, 1997).

This *BeppoSAX* project is still ongoing. We expect therefore to increase considerably the sample of soft X-ray selected BL Lacs for which we measure the spectrum in the 0.2–10 keV range and possibly above. With a larger complete sample, and combining the results with other complementary *BeppoSAX* projects, we expect to be able to draw a clearer picture of the relationship between the local X-ray slope and the overall energy distribution of this class of sources, in order to derive firmer conclusions on the behaviour at hard X-ray energies and on the mechanisms of the emission.

Acknowledgements. This work has received partial financial support from the Italian Space Agency (ASI contracts ASI 95/RS 72/SAX, and ASI ARS-96-70).

References

Bersanelli M., Bouchet P., Falomo R., Tanzi E.G., 1992, AJ, 104, 28 (B92)

Biermann P.L., Schaaf, R., Pietsch, W., Schmutzler, T., Witzel, A. & Kuhr, H., 1992, A&AS 96, 339 (Bi92)

Boella G., Butler R.C., Perola G.C., et al., 1997a, A&AS 122, 299

Boella G., Chiappetti L., Conti G., et al., 1997b, A&AS 122, 327

Bregman, J.N. 1990, A&ARev, 2, 125

Brinkmann W., & Siebert J., 1994, A&A 285, 812 (B94)

Brinkmann W., Siebert J., Reich W., Furst E., Reich P., Voges W., Trumper J., Wielebinski R., 1995, A&AS, 109, 147 (B95)

Butler C., Scarsi L., 1990, SPIE 1344, 46

Catanese, M. et al., 1997, ApJL, 487, L143

Catanese, M. et al., 1998, preprint, astro-ph/9712325

Ciliegi P., Bassani L. & Caroli E., 1995, ApJ 439, 80 (C95)

Comastri A., Molendi S., and Ghisellini, G. 1995, MNRAS, 277, 297

Dickey J.M. & Lockman F.J. 1990, ARAA, 28, 215

Edelson R., Pike G.F., Saken J.M., Kinney A., & Shull, J.M. 1992, ApJS 83, 1 (E92)

Elvis M., Wilkes, B.J., & Lockman, F.J., 1989, AJ, 97, 777

Falomo R., Bersanelli M., Bouchet P., Tanzi E.G., 1993, AJ, 106, 11 (F93)

Falomo R., Scarpa R., Bersanelli M., 1994, ApJS, 93, 125 (F94)

Gear W.K., 1993, MNRAS 264, 919 (G93)

Ghosh K.K. & Soundararajaperumal S., 1995, ApJS 100, 37 (GS95)

Giommi P., Barr P., Garilli B., Maccagni D. & Pollack A.M.T., 1990, ApJ 356, 432 (G90)

Giommi P., Ansari S.G., Micol A., 1995, A&AS, 109, 267 (G95)

Giommi P., Padovani P. & Perlman, E., 1998, To appear in “The Active X-ray Sky: Results from BeppoSAX and Rossi-XTE”, Nuclear Physics B Proceedings Supplements, L. Scarsi, H. Bradt, P. Giommi & F. Fiore (eds.), Elsevier Science B.V

Gregory P.C. & Condon J.J., 1991, ApJS 75, 1011 (GC91)

Griffith M.R., Wright A.E., Burke B.F. & Ekers R.D., 1995, ApJS, 97, 347 (Gr95)

Guainazzi M. & Matteuzzi A., 1997, SDC-TR 011

Hasinger G., Turner T.J., George I.M. & Boese G., 1992, Legacy, 2

Impey C.D., Neugebauer G., 1988, AJ, 95, 307 (IN88)

Impey C.D., Tapia S., 1988, ApJ, 333, 666 (IT88)

Isobe T., Feigelson E.D., Akritas M.G., and Babu G.J., 1990, Ap.J., 364, 104.

Jannuzzi, B.T., Smith, P.S., & Elston, R., 1993, ApJ 428, 130 (J94)

Kinney A.L., Bohlin R.C., Blades J.C & York D.G., 1991, ApJS 75, 645 (K91)

Lamer G., Brunner H. & Staubert R., 1996, A&A 311, 384 (L96)

Lanzetta K. M., Wolfe A.M. & Turnshek D.A., 1995, ApJ 440, 435 (L95)

Maraschi L., Ghisellini G., Treves A. & Tanzi E.G., 1986, APJ, 310, 325

Matt G., Guainazzi M., Frontera F. et al., 1997, A&A, 325, L13

Mazzarella J.M. & Balzano V.A., 1986, ApJS 62, 751 (MB86)

Mead A.R.G, Ballard K.R., Brand P.W.J.L, Hough J.H., Brindle C, Bailey J.A., 1990, A&AS 83, 183 (M90)

McNaron-Brown K. et al., 1995, ApJ, 451, 575 (MB95)

Nass P., Bade N., Kollgaard R.I., Laurent-Muehleisen S.A., Reimers D. & Voges W., 1996, A&A 309, 419 (N96)

Orr A. et al., 1998, To appear in “The Active X-ray Sky: Results from BeppoSAX and Rossi-XTE”, Nuclear Physics B Proceedings Supplements, L. Scarsi, H. Bradt, P. Giommi and F. Fiore (eds.), Elsevier Science B.V

Padovani P. & Giommi P., 1995, APJ, 444, 567

Padovani P. & Giommi P., 1995, MNRAS 277, 1477 (PG95)

Padovani P. & Giommi P., 1996, MNRAS, 279, 526

Padovani P., et al., 1998, To appear in “The Active X-ray Sky: Results from BeppoSAX and Rossi-XTE”, Nuclear Physics B Proceedings Supplements, L. Scarsi, H. Bradt, P. Giommi and F. Fiore (eds.), Elsevier Science B.V

Parmar A.N., Martin D.D.E., Baudaz M., et al., 1997, A&AS 122, 309.

Patnaik A. R., Browne I.W.A., Wilkinson P.N. & Wrobel J.M., 1992, MNRAS 254, 655 (P92)

Perlman E.S., Stocke J.T., Schachter, J.F., Elvis, M., Ellingson, E., Urry, C.M., Potter M., Impey C.D., Kolchinsky, P. 1996a, APJS, 104, 251 (P96a)

Perlman E.S., E.S. Stocke J.T., Wang Q.D. Morris S.L., 1996b, ApJ, 456, 451 (P96b)

Perlman E.S. & Stocke J.T., 1993, ApJ 406, 430 (PS93)

Pesce J.E., Falomo R., Treves A., 1994, AJ 107, 494 (P94)

Pian E., et al., 1998, ApJ, 492, L17

Pian E. & Treves A., 1993, ApJ, 416, 130 (Pi93)

Pian, E., Falomo, R., Scarpa, R., & Treves, A., 1994, ApJ 432, 547 (Pi94)

Punch, M., et al., 1992, Nature, 358, 477

Quinn J., et al., ApJ, 1996, 456, L83

Raiteri C.M., Villata M., De Francesco G., Lanteri L., Caval- lone M., Sobrito G., A&AS, 1998, (in press).

Remillard R.A., Tuohy I.R., Brissenden R.J.V., Buckley D.A.H., Schwartz D.A., Feigelson E.D. & Tapia S., 1989, ApJ 345, 140 (R89)

Sambruna R.M., Barr P., Giommi P., Maraschi L., Tagliaferri G., Treves A., 1994, ApJS, 95, 371 (Sa94)

Sambruna R.M., Maraschi L., and Urry C.M., 1996, ApJ, 463, 444.

Smith P.S., Jannuzi B.T., Elston R., 1991, ApJS 77, 67

Stecker O.C. & De Jager F.W., 1997, ApJ, 476, 712

Stocke J.T., Morris S.L., Gioia I.M., Maccacaro T., Schild R.E. & Wolter A., 1990, ApJ 348, 141 (S90)

Tovmassian H.M., Sherwood W.A., Sherwood V.E., Schultz G.V., Salter C.J. & Matthews H.E., 1984, A&AS 58, 317 (T84)

Ulrich, M.-H., Maraschi, L., and Urry, C.M., 1997, ARAA, n. 35.

Villata M., Raiteri C.M., Ghisellini G., et al., 1997, A&AS 121, 119

Villata M., Raiteri C.M., Lanteri L., Sobrito G., Cavallone M., 1998, A&AS, in press.

Wolter A., Caccianiga A., Della Ceca R., Maccacaro T., 1994, ApJ, 433, 29 (W94)

Worrall D.M., Wilkes B.J., 1990, ApJ, 360, 396 (WW90)